Trends Pharmacol. Drug Deliv., 2025, 1, Iss. 1, 21-38
DOI: 10.62184/tpdd.jtpdd110020241

Research article

Development of biodegradable chlorhexidine-functionalized polyurethane nanofibers for antimicrobial applications

Ahmed Abd El-Fattah[1,2,*], Hend Ramadan[1], Labiba El-Khordagui[3] and Sherif Kandil[1]

[1] *Department of Materials Science, Institute of Graduate Studies and Research, Alexandria University, El-Shatby, 21526, Alexandria, Egypt*
[2] *Department of Chemistry, College of Science, University of Bahrain, P.O. Box 32038, Sakhir, Kingdom of Bahrain*
[3] *Department of Pharmaceutics, Faculty of Pharmacy, Alexandria University*

Received: 26 July 2024
Revised: 11 November 2024
Accepted: 14 November 2024
Published: 17 February 2025

Keywords:

Chlorhexidine, nanofibers, polyurethane, cytocompatibility, drug release

Corresponding author*:
Ahmed Abd El-Fattah,
Email: a_abdelfattah@alexu.edu.eg

Abstract: Conventional chlorhexidine (CHX) formulations provide a short-term antibacterial effect which necessitates repeated application with compromised patient compliance. There is an unmet demand for controlling CHX delivery at local infections or operative sites to comply with specific therapeutic needs. We propose herein CHX-functionalized nanofibers (NFs) fabricated using a series of poly(ethylene glycol)-poly(caprolactone) (PEGCL) amphiphilic copolymers with different molecular weight (MW) and hydrophilicity as an approach to sustaining CHX release. Physicochemical characterization indicated poly(ether-ester-urethane) structures with different MW (85450-338400), relatively high water uptake capacity (150-230 % at 6 h), biodegradability, and cytocompatibility. Electrospinning of organic copolymer solutions containing 0.5 % CHX resulted in NFs with a 263-205 nm mean diameter, 77.3-85.4 % entrapment efficiency, and molecular drug distribution with no discernible drug-copolymer interaction. Drug release from NFs at pH 7.4 and pH 4.5 took place according to different patterns depending mainly on the copolymer MW, hydrophilicity, and content of the PEG segment as well as the medium pH. Multi-hour to multi-day CHX release could be achieved featuring a range of burst and sustained release phases to meet antimicrobial needs ranging from immediate short-term effects at higher drug concentrations to sustained antimicrobial effects in longer-term applications.

1. Introduction

The increase of antimicrobial resistance (AMR) associated with reduced effectiveness of antibiotic-based prevention and treatment of infections is a heavy global health and financial burden [1]. This created an urgent demand for non-antibiotic ternatives for antimicrobial biomedical applications. A wide array of non-antibiotic anti-infectives including synthetic agents [2], inorganic nanomaterials [3] and natural actives derived from plant [4], marine [5], and microbial [6] origins are currently under active investigation.

Among synthetic antibacterials, chlorhexidine (CHX) is a broad-spectrum and fast-acting anti-infective with documented bactericidal activity at concentrations used in clinical settings and the ability to inhibit biofilms formed by different bacterial species [7]. Additionally, CHX does not reduce the sensitivity of common microbes [8]. Owing to the cationic properties of the CHX bis-biguanide molecule (Figure 1S) at physiological pH, it interacts with the negatively charged bacterial cells, resulting in cell membrane damage and leakage of the cytoplasm. As an effective disinfectant, CHX is widely used in preventing surgical skin infections and cleaning wounds [9] as well as sterilizing surgical tools [10, 11]. The drug is the most commonly used anti-infective agent in operative dentistry and endodontics [12, 13]. Moreover, CHX is widely used in personal healthcare products, such as hand and mouth washing solutions and related formulations [14-16].

Conventional CHX formulations usually provide short-term antibacterial efficacy which necessitates repeated application, reducing patient compliance. Controlling CHX delivery at the

required site according to a pattern appropriate for specific therapeutic needs would support a sustained antimicrobial action. In this context, CHX delivery systems have been developed using a wide range of biomaterials such as hydrogels [16, 17], polymer nanoparticles [18], inorganic nanomaterials [19, 20], clay nanotubes [21] and foam [16].

In recent years, electrospun nanofibers (NFs) have gained growing attention as drug delivery and regenerative highly porous matrices characterized by a large surface area and tunable physicochemical and mechanical properties [22, 23]. Polymer NFs greatly advanced the biomedical applications of CHX, particularly those involving controlled delivery of the drug in dentistry to fill infected voids as well as other applications [24, 25]. Furthermore, CHX-NFs were used in anti-infective / guided tissue regeneration and wound healing applications [26, 27].

Several strategies have been adopted to customize CHX release from NFs as a main determinant of their antibacterial functionality. These include mainly increasing CHX loading [28-30], cross-linking [27, 31], engineering NF matrix as bilayer [32], as well as fusing NF as hydrogels [27, 31]. An alternative effective approach involves the electrospinning of polymer combinations either as physical polymer blends or core-shell and block copolymer structures [33, 34]. However, attempts to utilize block copolymers as a strategy for modulating CHX release from NFs are scarce to date [30, 35] and such an approach would enrich the non-antibiotic NFs platform with CHX-NFs with different physicochemical properties and drug release patterns.

Kasbiyan et al. [30] prepared electrospun nanofibers with antibacterial properties derived from γ-polyglutamic acid (γ-PGA) and loaded with CHX and triclosan (TCS) as antibacterial agents. The morphology of the electrospun nanofibers was significantly modified after the crosslinking reaction with cystamine, increasing their diameter and surface roughness according to the amount of the added crosslinker. Release rates were clearly dependent on the hydrophilicity of the selected drug, the characteristics of the release medium, and the crosslinking degree.

Amphiphilic copolymer-based nanofibers present a versatile platform for drug delivery, offering advantages such as high drug loading capacity, controlled and sustained release, biocompatibility, ease of fabrication, and the potential for targeting specific sites within the body. These properties make them an attractive choice for advancing drug delivery technologies, especially for complex diseases requiring precise treatment strategies [34, 36].

The aim of the present study was to utilize a copolymer-based approach for the development of CHX-functionalized polyurethane NFs with customizable CHX release for local antimicrobial applications. The study involves the synthesis and characterization of a series of amphiphilic poly(ethylene glycol)-poly(caprolactone) (PEGCL) copolymers with different compositions and molecular weights for the electrospinning of antimicrobial CHX-NFs with tunable physicochemical characteristics and drug release patterns.

2. Materials and Methods

2.1. Materials

All reagents were purchased from El-Gomhoria Co., Egypt unless otherwise noted. CHX base was prepared from CHX acetate followed by double crystallization. Dichloroethane (DCE) was dried by refluxing over calcium hydride for 4 h and then distilled under a dry nitrogen atmosphere prior to use. Toluene was refluxed over sodium and distilled before use. *N,N*-dimethylformamide (DMF), tetrahydrofuran (THF), diethyl ether, and methanol were used as received without further purification. 1,6-Hexamethylendiisocyanate (HMDI) obtained from Aldrich Chemical Co., Germany was distilled at reduced pressure (90 ºC/ 1 mm Hg). Tin(II) octoate, $Sn(Oct)_2$ (Aldrich Chemical Co., Germany) was used as received. Poly(ethylene glycol), PEG, (MW 2000, 3400) and poly(ε-caprolactone). PCL-diol (MW 2000) supplied by Aldrich Chemical Co., Germany were dried by azeotropic distillation with toluene and dried under vacuum.

2.2. Synthesis of polyethylene glycol polycaprolactone copolymers (PEGCL)

The poly(ether ester urethane) copolymers (PEG/CL) were synthesized by a one-step condensation reaction [36] according to the synthetic pathway schematically described in Figure 1.

The macrodiol prepolymers PEG (Mw 2000 or 3400) and PCL-diol (MW 2000) in different ratios (Table 1) were dissolved in dry toluene under a dry nitrogen atmosphere to obtain a concentrated solution (15% w/v). Stoichiometric amounts of HMDI as chain extender and $Sn(Oct)_2$ as catalyst were added and the reaction was allowed to proceed for 7 h at 70°C. The copolymers were obtained in high yields (≥95%) by precipitating

the reaction mixtures using an excess of low-boiling petroleum ether. For purification, the copolymers were separated, dissolved in chloroform, reprecipitated in diethyl ether, and finally dried under vacuum at room temperature for at least 48 h. The chemical composition and MW of the macrodiols used in the preparation of PEGCL copolymers and the feed molar ratios used in their synthesis are shown in Table 1.

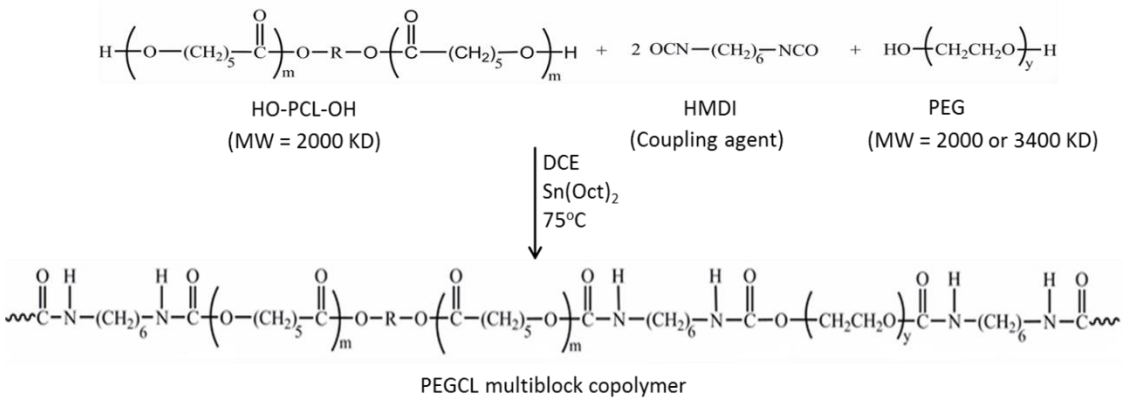

Figure 1. Scheme for the synthesis of PEGCL multiblock copolymer.

2.3. Characterization of polyethylene glycol-polycaprolactone copolymers

The FT-IR analysis was performed using a Perkin-Elmer FT-IR spectrometer, from 4000 to 600 cm^{-1}. The spectra were taken as averages of 16 scans at a resolution of 4 cm^{-1}. The samples were prepared as polymer cast films on KBr plates obtained from slowly evaporated chloroform solutions (0.5% w/v). The ^{1}H-NMR spectra were recorded on a Varian Gemini 200 spectrometer operating at 200 MHz, using chloroform-d ($CDCl_3$) as solvent and tetramethylsilane (TMS) as internal standard. Size exclusion chromatography (SEC) analyses were performed on an Agilent 1100 Series HPLC system (Agilent Technologies, Waldbronn, Germany) utilizing three PLgel columns (7.5 × 300 mm, with 5 µm particle size and a 100 Å pore size). The system was equipped with a quaternary pump, and autosampler, and connected with a diode array detector (DAD). The mobile phase was THF flowing at a rate of 1.0 ml/min and the calibration curve was constructed by using mono-dispersed polystyrene standards.

Table 1. Synthesis of poly(ether-ester-urethane) derived from PEG and PCL-diol with HMDI as a junction unit.

Sample Code[1]	PEG			PCL-diol			HMDI	
	(M_n)	(mmol)	(g)	(M_n)	(mmol)	(g)	(mmol)	(g)
PEGCL-I-25	2000	1	2.0	2000	3	6	4	0.67
PEGCL-I-50	2000	1	2.0	2000	1	2	2	0.33
PEGCL-I-75	2000	3	6.0	2000	1	2	4	0.67
PEGCL-II-25	3400	1	3.4	2000	3	6	4	0.67
PEGCL-II-50	3400	1	3.4	2000	1	2	2	0.33
PEGCL-II-75	3400	3	10.2	2000	1	2	4	0.67

[1]Codes denote the MW of PEG (I=2000, II=3400) and the mol % of PEG (25, 50, and 75).

Differential scanning calorimetry (DSC) measurements were performed using a Mettler TA 4000 instrument under a nitrogen atmosphere using 10-15 mg samples. These were submitted to a first heating scan from 30 °C to 100 °C at a heating rate of 10 °C/min and then cooled from 100 °C to -100 °C at a cooling rate of 10 °C/min, followed by 4 min of isotherm. The second heating scan was run from -100 °C to 100 °C at a heating rate of 10 °C/min. The melting temperatures (Tm) were taken as the maximum at the peak of the melting endotherms. Wide angle X-ray diffraction (WAXD) patterns were recorded using nickel-filtered Cu K_α radiation produced by an X-ray 7000 Shimadzu diffractometer operated at 40 kV and 180 mA in the 2θ scanning mode between 5 and 35 °C. Static contact angle measurements were performed on polyurethane films spin-coated from chloroform solutions at 25 ± 0.1 °C with a DSA 10 drop shape analysis system (Kruss, Hamburg, Germany). Contact angles were measured by placing a 5 µl droplet of Milli-Q water on the sample surface. The data presented are averages of 10 measurements.

The cytotoxicity of a representative copolymer (PEGCL-I-25) was assessed using 3T3/A31 fibroblasts and fluid extract of the copolymer and copolymer-free control [37]. The extract was obtained by incubating the copolymer specimens 20 mg/ml in Dulbecco's Modified Eagle Medium (DMEM) for 48 h at 37 °C and used either undiluted or at 1:2 and 1:4 dilution ratios in DMEM. A subconfluent monolayer of fibroblasts was trypsinized using a 0.25% trypsin in a 1mM EDTA solution. Cells were centrifuged at 1000 rpm for 5 min, then resuspended in full DMEM media and counted. Dilutions were made to achieve 3 x 10^3 cells per 100 µl of media in each well of 96-microwell plates. Plates were incubated at 37°C in a 5% CO_2 environment for 24 h until 60-70% cell confluence was achieved. The medium was replaced with the copolymer extract. After 24 h of incubation, cells were treated with WST-1 cell proliferation reagent diluted at 1:10 for 4 h at 37°C in 5% CO_2, and the absorbance was measured at 620 nm using a Benchmark Bio-Rad Microplate Reader to determine the number of viable cells. Data was processed using Microplate Manager III (Bio-Rad) and Igor Pro (Wave-metrics), n = 3.

2.4. Plain copolymer (PEGCL) nanofibers

2.4.1. Preparation of plain PEGCL nanofibers

Plain nanofibers (NFs) of the four selected copolymers, PEGCL-I-25, PEGCL-I-50, PEGCL-II-25, PEGCL-II-50 (Table 1) were prepared by the electrospinning of an organic solution of the copolymer using an electrospinning apparatus equipped with a high voltage DC power supply. The polymer solution was filled in a 10-ml syringe fitted with a metallic needle with an internal diameter of 0.88 mm connected to a positive electrode. The syringe was connected to a syringe pump to control the flow rate. The needle was horizontally aligned with a copper collector plate covered with aluminum foil. Fabrication of NFs was performed at an ambient temperature of ~25 °C and relative humidity < 65%. The collected NFs were dried overnight under vacuum.

The effect of key process and formulation variables on the electrospinnability of the organic copolymer solutions was assessed using one-factor-at-a-time experiments. Electrospinnability was judged by the reproducible formation of a defect-free mesh of beadless nanoscale continuous and uniform NFs by scanning electron microscopy (SEM). Formulation variables included organic solvent composition (DCM, $CHCl_3$, and DCM/DMF blend 4: 1) and copolymer solution concentration (5 and 10% w/v) while process variables included voltage (20, 25, and 30 kV), copolymer solution flow rate (0.125, 0.25 and 0.5 mL/h) and spinneret to collector distance (10, 15 and 20 cm).

2.4.2. Characterization of plain PEGCL nanofibers

The morphology of the plain electrospun PEGCL NFs was determined by high resolution SEM, (JSM-5300, JEOL, Japan). Samples of NFs were gold-coated with an ion sputtering coater (JFC-1100E, JEOL, Japan) and examined with an accelerating voltage of 25 or 20 kV. Images were also used to measure the diameter of NFs (100 random measurements) using Digimizer 4® image software.

The water uptake capacity of the PEGCL NF meshes in comparison with PCL-diol NFs prepared using a 10% w/v copolymer solution was determined gravimetrically at 37°C. The initial weight (W_0) of 2 x 2 cm samples (~ 0.1 g) of the dried NF meshes was recorded and the samples were immersed in 10 ml distilled water at 37°C. At predetermined time intervals (1, 2, 3, 4, 5, and 24 h), the samples were removed from water, gently blotted with a filter paper, weighed (Wt), and re-immersed in the buffer. Water uptake (%) was calculated using the following formula, equation **(1)**, [38], n = 3:

$$\textbf{Water Uptake}\ (\%) = \frac{W_0 - Wt}{W_0} \times 100 \qquad (1)$$

The hydrolytic degradation of the PEGCL NFs in comparison with PCL-diol NFs was determined by calculating the weight loss of NFs upon fully immersing a known weight of dried samples (W_0, 0.1g approximately) in 10 ml of phosphate buffer saline (PBS, pH 7.4) in sealed falcon tubes at 37°C in a constant temperature incubator. At predetermined time intervals (1, 2, 3, 7, 14, 28, and 35 days), samples were removed, rinsed several times with deionized water, and dried under vacuum for 3 days. The remaining weight (Wt) was determined, and the % weight loss was calculated as follows in equation **(2)**:

$$\textbf{Weight Loss}\ (\%) = \frac{\mathbf{W_0 - Wt}}{\mathbf{W_0}} \times \mathbf{100} \qquad \textbf{(2)}$$

In addition, SEM analysis was performed on the degraded samples at 6 weeks to assess the change in morphological characteristics.

2.5. Chlorhexidine loaded copolymer (CHX-PEGCL) nanofibers

2.5.1. Preparation of CHX-PEGCL NFs nanofibers

These were fabricated by electrospinning as described above. Briefly, the copolymers were dissolved in a DCM/DMF solvent blend (4: 1) to obtain a 10% w/v solution of PEGCL-I-25 and PEGCL-I-50 and 5% w/v solution of PEGCL-II-25 and PEGCL-II-50. The concentration of the CHX base was 0.5% of the polymer mass. Electrospinning was performed at 20 kV, 0.25 ml/h copolymer solution flow rate, and 10 cm spinneret to collector distance. The NF mats obtained were stored at ambient temperature protected from light and humidity.

2.5.2. Characterization of CHX-PEGCL NFs nanofibers

The NF morphology was examined by high resolution SEM and the mean fiber diameter was determined as described above. The FT-IR scans of samples of CHX, plain PEGCL NFs, and CHX-PEGCL NFs prepared in potassium bromide (KBr) discs were obtained in the wave number range 500 to 4000 cm^{-1} as described under section 2.3. In addition, DCS traces of CHX, plain PEGCL NFs and CHX-PEGCL NFs and physical mixtures of the components in amounts equivalent to the ratios present in the NFs were recorded between 30 to 200 ºC, at a heating rate of 10 ºC/min (DSC-6, CT, PerkinElmer instruments, USA). Inert atmosphere was maintained by purging nitrogen at a flow rate of 20 ml/min. A control empty pan was subjected to the same conditions.

The entrapment efficiency (EE %) of CHX base was assessed by determining the drug content of NFs following extraction by vortex mixing accurately weighed NF samples (26 mg) in 100 ml of acetate buffer pH 4.7 for 5 min. The aqueous drug extracts were filtered through Whatman filter paper, and the clear solutions were analyzed for CHX content spectrophotometrically at λ_{max} 260 nm (n = 3). A similarly prepared solution using plain NFs was used as blank. The EE% was calculated as follows in equation **(3)**:

$$\textbf{EE}\ (\%) = \frac{\textbf{Actual drug loading}}{\textbf{Theoretical drug loading}} \times \mathbf{100} \qquad \textbf{(3)}$$

2.5.3. Chlorhexidine release from PEGCL nanofibers

The release of CHX from NFs was examined in 0.1 M PBS, pH 7.4 and acetate buffer pH 4.7. Strips of NFs weighing approximately 0.1 g were immersed in 10 ml of the release medium in 20 ml-capped vials in a shaking water bath at 37ºC. At predetermined time intervals, 1 ml-sample of the release medium was withdrawn and replaced with an equal volume of fresh medium at 37°C. The concentration of released CHX was measured spectrophotometrically at λ_{max} 260 nm using a preconstructed calibration graph, n = 3.

2.6. Statistical analysis

Experiments were run in triplicate for each sample. Data were presented as the mean ± standard deviation (SD). Results were analyzed by Student's t-test. Values of $p \leq 0.05$ indicated statistical significance.

3. Results and discussion

Figure 1 depicts the schematic synthesis of PEGCL multiblock copolymers with various compositions (Table 1). The polymerisation process involves a one-step condensation reaction between the -NCO groups of the chain extender HMDI and the main -OH groups of the diols (PEG and PCL), which results in the production of urethane groups along the polymeric backbone. Because water can react with HMDI to produce carbamic acids and hence inhibits polymerisation. the process was carried out under extremely anhydrous conditions and in a nitrogen environment. Although no small molecules such as water or carbon dioxide are removed during polymerisation, the reaction between diol and diisocyanate to generate linear copolymers can be identified as condensation polymerisation [36].

DOI: 10.62184/tpdd.jtpdd110020241

3.1. Physicochemical characteristics of the PEGCL multiblock copolymers

Structural characteristics of the copolymers were verified by FT-IR and NMR spectroscopic analysis (Figure 2A and B, respectively). FT-IR spectra of three representative PEGCL copolymers in addition to PEG and PCL are shown in Figure 2A. The PEG spectrum showed an absorption band at 1107 cm^{-1} attributed to the stretching vibration of the –C–O–C– which appeared in the spectra of copolymers with increasing intensity as a function of PEG content and length of the PEG segment as reported [39]. For PCL, the characteristic C=O stretching vibration peak of the ester carbonyl group at 1756 cm^{-1} was observed in PEGCL spectra at 1732–1696 cm^{-1} indicating hydrogen bonding between the urethane bond and PCL or PEG [40].

The ^{1}H-NMR spectrum of a representative copolymer PEGCL-I-50 (Figure 2B) showed the characteristic peaks of both PEG (sharp singlet at 3.63 ppm due to CH_2CH_2 protons) and PCL (two equally intense triplets at 4.05 and 2.30 ppm attributed to the CH_2 units) [41]. In addition, ^{1}H NMR data for all copolymers were used to evaluate their composition relative to the feed ratio by integrating the intensity ratio of the methylene protons (–OCH_2CH_2–: δ=3.65) in the case of PEG and the methylene protons (–(CH_2) 3–: δ=4.05) in the ε–caprolactone unit of PCL. Compositional data (Table 1S) were generally consistent with the starting prepolymer feed molar ratios. The table also shows the weight average molecular weight (MW) and polydispersity (MW/Mn) of PEGCL copolymers measured by SEC.

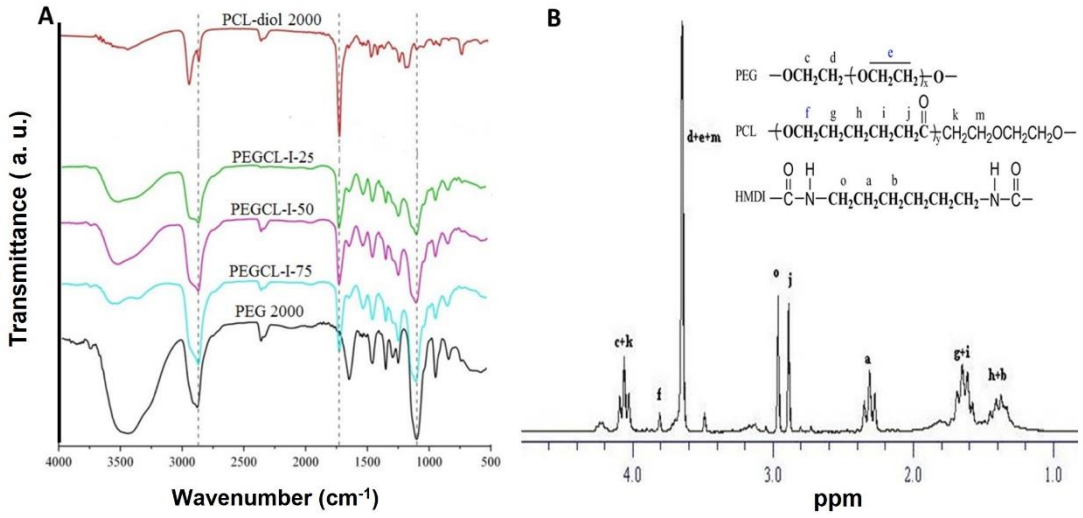

Figure 2. Copolymer characterization: (A) FT-IR spectra of selected samples and (B) ^{1}H-NMR spectrum of a representative copolymer, PEGCL-I-50.

Solid state properties of the copolymers in comparison to their PEG and PCL-diol prepolymers including DSC and WXRD patterns are shown in Figure 3A and B, respectively. The PEG 2000 thermogram (PEGCL-I) showed one peak at 62°C while PCL-diol showed two melting temperatures (T_m) at 52 °C and 57 °C [42, 43]. The PEGCL copolymers showed only one peak and T_m values were slightly lower than that of PCL-diol. In addition, their areas were smaller than that of both soft and hard segments indicating lower crystallinity of copolymers. In the PEGCL-I series, T_m values varied between 42°C and 51°C and were not influenced by the change in PEG segment size. On the other hand, DSC traces of the PEGCL-II series revealed an increase of T_m with the increase in PEG segment size.

As indicated by WAXD patterns of PEGCL copolymers (Figure 3B), a crystalline phase of the PEG and PCL blocks was evident by the appearance of sharp characteristic peaks at 2θ of 19.4° and 23.7° for PEG as well as 21.7° and 24.0° 2θ for PCL [43].

DOI: 10.62184/tpdd.jtpdd110020241

Patterns for PEGCL-I-25, PEGCL-I-50, and PEGCL-II-25 indicated enhanced crystallinity of PCL blocks and the amorphous nature of PEG. On the other hand, PEGCL-I-75, PEGCL-II-50, and PEGCL-II-75 patterns revealed PEG crystallization. When comparing PEGCL-II-50 to PEGCL-I-50, the lack of PCL crystallization suggested that there was a PCL MW threshold below which PCL domains could not crystallize when PEG domains were present, which was consistent with DSC data [42].

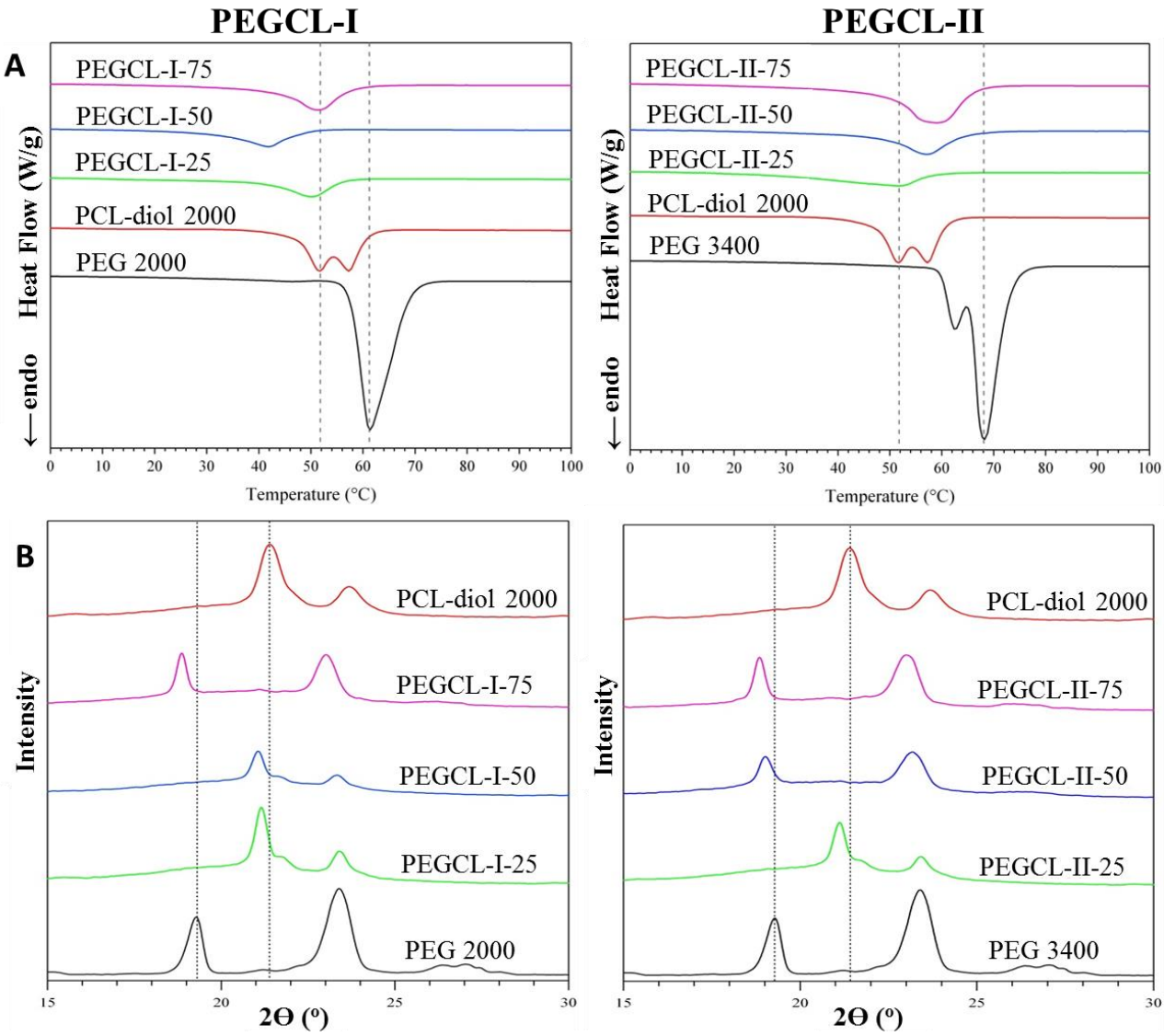

Figure 3. Solid state properties of PEGCL copolymers (PEGCL-I and PEGCL-II) based on PEG and PCL macrodiols: (A) DSC thermograms and (B) WAXD patterns.

Table 2 displays the values of static contact angle θ (theta) measured for PEGCL copolymers. The PEGCL-II-75 copolymer with 75% PEG (MW 3400) has a less hydrophobic surface, with a contact angle approximating 30 ± 1.4°. Copolymers with a lower 25 and 50% PEG content (PEG (MW 2000 and 3400), had average contact angle values of 72 ± 2.8° and 68 ± 2.1°, respectively. The MW of PEG utilized had no significant effect on this composition. In several cases, materials that absorb water may not necessarily have lower contact angles. Such variances may be attributed to individual disparities in the surface roughness of the films, as well as the existence of defects such as pinholes or microcracks generated during solvent evaporation [44].

3.2. Biological activity of a representative PEGCL copolymer

The cytotoxicity of the representative PEGCL-I-25 copolymer was determined in the form of a fluid extract as reported [37]. The effect of the extract in three concentrations, 25, 50, and 100 %, was assessed using a 3T3/Balb clone A31 mouse embryo fibroblast cell line following 24 h-incubation. As shown in Figure 4, cell viability was not significantly affected by the copolymer extract at all concentrations (p> 0.05), indicating potential cytocompatibility of the PEGCL copolymers.

According to data obtained, the synthesized copolymers have different MW as well as different proportions and MW of PEG segment, water absorption capacity, biodegradability, and biocompatibility which justified provisional suitability as biomaterials for diverse biomedical applications.

3.3. Electrospun copolymer nanofibers

3.3.1. Factors affect nanofibers morphology and structure

The PEGCL-I-25 and PEGCL-I-50 (10% w/v) and PEGCL-1I-25, and PEGCL-1I-50 (5% w/v) copolymers were electrospun and characterized as plain nanofibrous scaffolds prior to CHX loading and release. Judging by high resolution SEM imaging of the NFs (Supplementary Figures 2-5), the processing and formulation variables known to affect the morphological properties of NFs [33] were adjusted as follows: 20 kV, 0.125 ml/h flow rate, and 10 cm spinneret-collector distance using DCM/DMF 4: 1 as solvent. The mean NF diameter ranged from 82 to 117 nm (Table 3).

The optimized copolymer NFs were further characterized for water uptake and biodegradability at 37 ºC. As shown in Figure 5A, water uptake was considerably affected by the copolymer composition resulting in different water absorption rates prior to equilibrium which was reached at 6 h approximately in all cases and maintained throughout the 24 h-study period. Water uptake by the NFs of the prepolymer PCL-2000 used for comparison was minimal due to the lack of the soft hydrophilic PEG moiety. Values for the % water uptake at 6 h reflected bulk hydrophilicity and the content of PEG segments. For instance, PEGCL-I-25 and PEGCL-II-25 NFs displayed lower water uptake (150% and 180%, respectively) because of a lower proportion of PEG segments leading to limited chain mobility and poorer intrusion of water molecules into the NFs structure [45]. On the other hand, PEGCL-I-50 and PEGCL-II-50 copolymers with a larger proportion of PEG segments exhibited greater water sorption (170% and 230%, respectively) attributed to higher bulk hydrophilicity due to a greater content of PEG segment hydrophilicity and chain flexibility [46].

Biodegradation of the copolymer NFs expressed as the % weight loss versus time in PBS pH 7.4 at 37ºC is depicted in Figure 5B for PEGCL-I and PEGCL-II copolymers, respectively. The copolymers with a larger proportion of hydrophilic PEG segments underwent a greater extent of weight loss irrespective of their molecular weights corroborating their water uptake and bulk hydrophilicity data (Figure 5A) and those for other PEG-based copolymers [46]. In fact, faster intrusion of water molecules into NFs with larger PEG content enhances biodegradation which leads to increased NFs porosity and further matrix degradation [47]. Random hydrolysis of the PEG-C-PCL in the backbone chain accounts for the weight loss of these copolymers.

Morphological and structural changes, monitored by SEM at 3 days and 24 days (Figure 6 A and B, respectively) verified weight loss data. However, copolymer NFs retained partial structural integrity of relatively large matrix fragments throughout the degradation study.

Table 2. Static contact angles of PEGCL copolymers spin-coated films (data averaged over 10 measurements).

Copolymer	PECL-I-25	PECL-I-50	PECL-I-75	PECL-II-25	PECL-II-50	PECL-II-75
Contact Angle (θ)	78 ± 2.5	72 ± 1.8	45 ± 3.1	68 ± 3.1	64 ± 2.2	30 ± 1.4

DOI: 10.62184/tpdd.jtpdd110020241

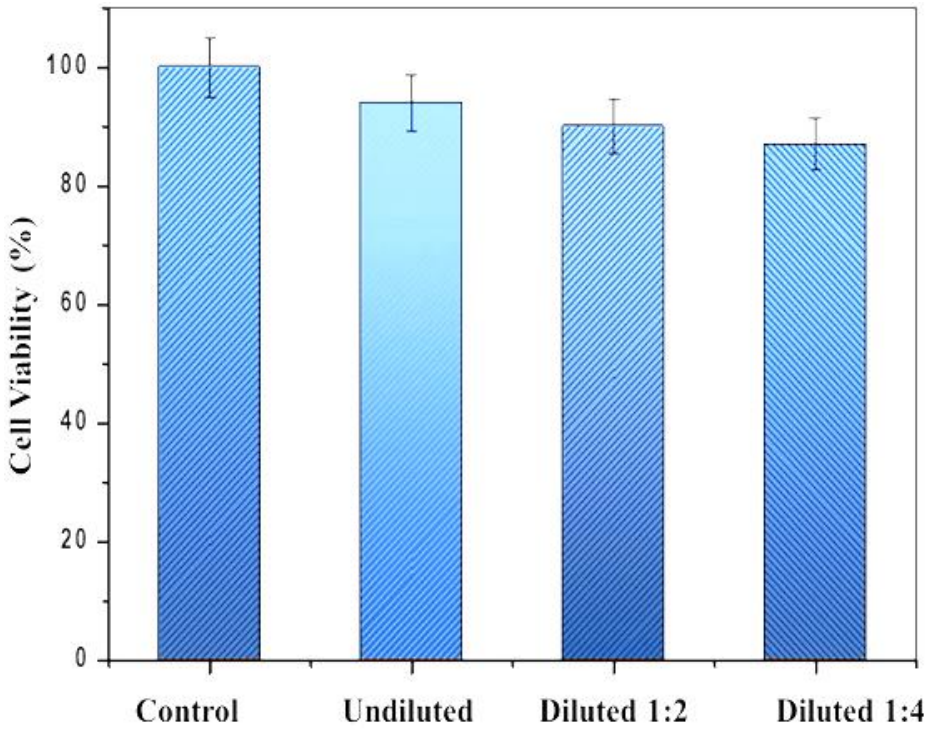

Figure 4. In vitro cytotoxicity of a representative copolymer (PEGCL-I-25) using 3T3/Balb clone A31 mouse embryo fibroblast cells following 24 h exposure. Values are the means ± SD (n=3).

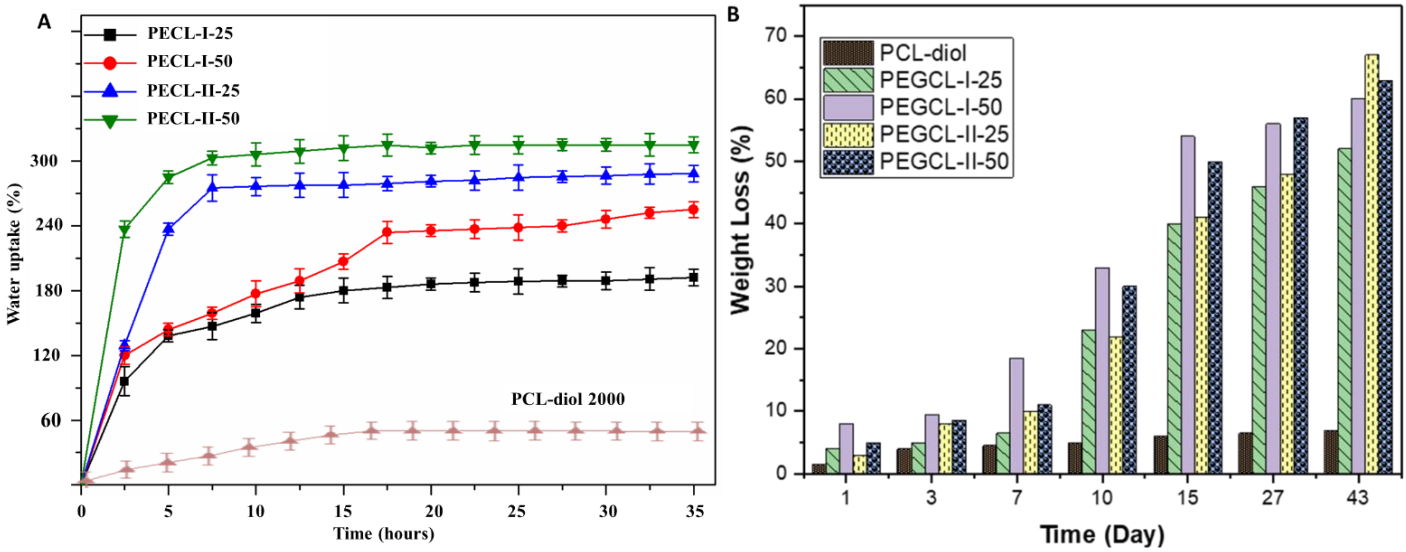

Figure 5. Properties of plain copolymer nanofibers relative to PCL-diol (2000) prepolymer nanofibers at 37°C: (A) Water uptake capacity; (B) Weight loss (%).

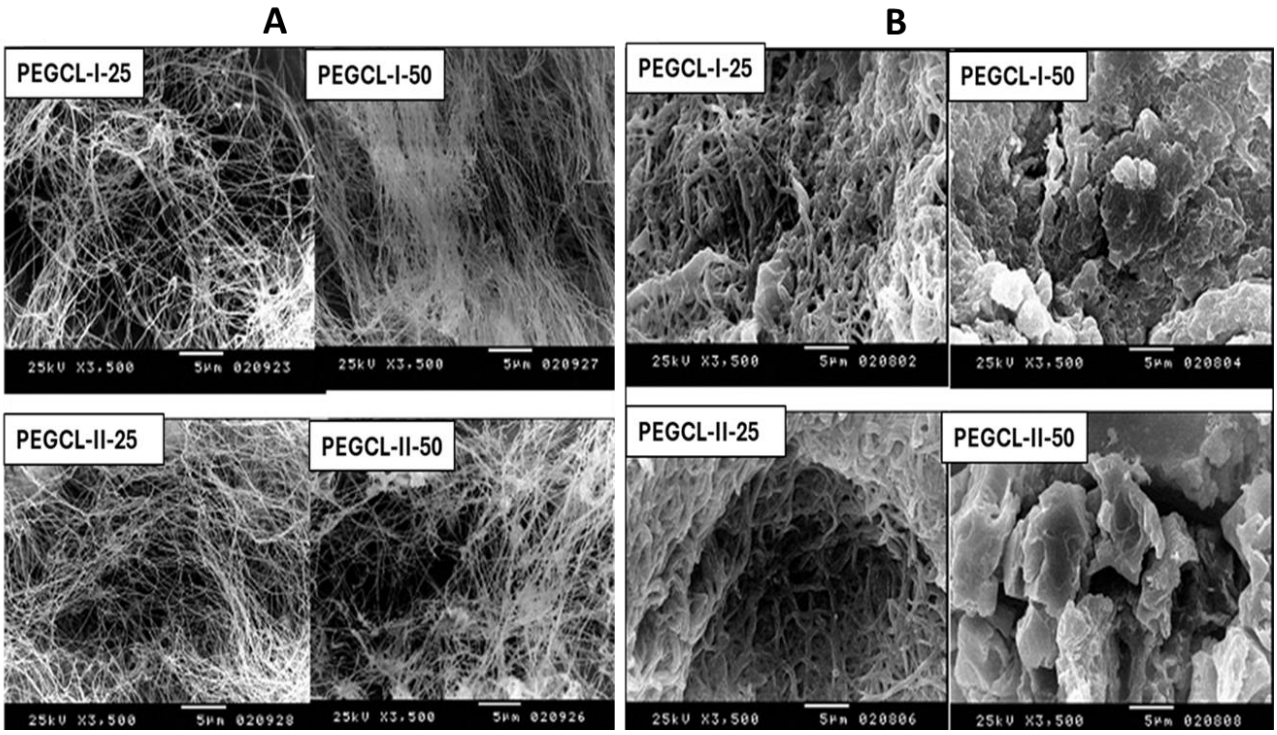

Figure 6. SEM for the degradation of plain copolymer nanofibers in PBS pH 7.4 at 37ºC for: (A) 3 days and (B) 42 days.

3.3.2. Chlorhexidine-loaded copolymer nanofibers

The copolymer NFs were loaded with CHX to generate four NFs formulations with 5 and 10% w/v copolymer concentration and containing 0.5% w/w CHX (Table 3). This concentration is within the range of CHX concentration in NF formulations [29, 48] for potential use in antimicrobial/regenerative applications. Electrospinning of CHX/copolymer NFs was undertaken under the adjusted conditions described above. As shown by SEM imaging at two magnification powers (Figure 7A and B, respectively), NFs were continuous and junction-free with a mean diameter ranging from 163 to 205 nm. All NFs exhibited a smooth surface with no surface-deposited CHX crystals indicating homogeneous incorporation of the hydrophobic drug molecules within the NFs, due to CHX solubility in the DCM/DMF solvent blend. In general, phase separation does not take place upon jet thinning and solvent evaporation when the drug is compatible with the polymer and solvent system [46, 49]. The relatively high EE% of CHX by all NFs (77.3 - 85.4 %, Table 3) verified effective drug incorporation.

Data for solid state properties of CHX-copolymer NFs (CHX-NFs) in comparison with their CHX and copolymer components including FT-IR and XRD are shown in Figure 8A and B, respectively. The FT-IR spectrum of CHX showed characteristic absorption bands at 3358.8 cm^{-1} and 3442.7 cm^{-1} attributed to N–H stretching vibration and bands at 1610 cm^{-1} and 1489 cm^{-1} assigned to C = C aromatic bending. Peaks at 1650, 1600, 1550, and 1500 cm^{-1} indicated C = C stretching of the CHX aromatic moiety [50, 51]. The spectra for PEGCL NFs showed a very sharp band around 3400 cm^{-1} assigned to N–H stretching and an absorption peak around 1720 cm^{-1} due to the C=O groups in poly (ester urethane). Other details were discussed under FT-IR characterization of copolymers (Section 3.1). Spectra of CHX-NFs showed characteristic peaks of CHX and the copolymers. However, the disappearance of CHX bands at 3062.8 cm^{-1}, 1885.3 cm^{-1}, 1395.4 cm^{-1}, and 770.51 cm^{-1} as a result of possible physical interaction between CHX and the copolymer matrices could be observed.

As illustrated in Figure 8B for DSC data for CHX-NFs and their components, the CHX curve exhibited two melting points depicted as a small peak at 122.04 °C and a large peak extending from 129.7°C (onset) to 138.81°C (endset). Sharp melting transition of CHX was observed at 133.9°C after which a sequential thermal decomposition process took place [52]. The thermograms of plain PEGCL polymeric NFs showed a smooth curve over the range 30-200ºC with a major endothermic peak in

the range 45-50 ºC corresponding to the melting temperature of the copolymer. The melting peaks of these NFs were in the range of 47.9 to 50.4°C. Thermograms of plain NFs were similar to those of their corresponding PEGCL copolymers (Figure 3A) implying lack of an electrospinning effect on the thermal behavior of the copolymers. For CHX-copolymer NFs, the disappearance of the large meting peak of CHX suggested possible physical interaction preventing melting of the drug and promoting molecular dispersion of the drug [53]. Slight changes in the peaks' shape and height-to-width ratio can be attributed to possible differences in the sample mixture geometry [54].

The FT-IR and DSC characteristics of the CHX-NFs provided evidence for the lack of chemical interaction between the drug and polymer matrix, an observation of importance in developing NF-based polyurethane NFs not impeding CHX release.

3.3.3. Chlorhexidine release

The release of CHX from NFs containing 0.5% of the drug in PBS pH 7.4 and acetate buffer pH 4.7 at 37ºC (Figure 9A and B, respectively) was investigated for 42 days and 6 hours, respectively to compare the carrier properties of the four copolymers and their suitability for different local antimicrobial applications. The release patterns of CHX were different in the two-release media, being much faster at the slightly acidic pH 4.7 usually encountered in the acid mantle of the skin surface [55].

Drug release from copolymer NFs at a certain drug content can be affected by multiple factors related to the physicochemical properties of the drug, copolymer matrix and the electrospun NFs [46, 47, 56]. Drug properties include mainly MW, crystallinity, compatibility with the polymer matrix, drug-polymer interactions and solubility in the release medium. The copolymer matrix may affect drug release via its MW, crystallinity, proportion and MW of hydrophilic component, water uptake and biodegradability while the nanofibrous structure may modulate drug release depending on its thickness, porosity, specific surface area, entanglement, and NF orientation. Finally, the release environment including composition, pH, temperature and added surfactants, solvents or enzymes may greatly modify release kinetics. As indicated by characterization data (Figure 5), CHX is physically compatible with the copolymer matrix with a tendency for localization within the hydrophobic core of the NFs with no chemical interaction with the NF matrix.

The CHX release profiles at physiological pH (Figure 9A) were generally biphasic, encompassing a relatively fast burst phase attributed to release of the drug near or deposited on the NFs surface and a slower sustained release phase of the drug in the hydrophobic core. The % cumulative CHX release at 2 days was in the order: PEGCL-1-50 (98%) > PEGCL-1I-25 (80%) > PEGCL-I-25 (63%) > PEGCL-II-50 (58%). Moreover, CHX release from PEGCL-I-25 and PEFCL-II-50 was sustained for more than 40 days. Data for the four copolymer NFs indicated general dependence of CHX release on the copolymer MW (Table 3). For copolymers with the same MW of the PEG segment (2000) and copolymer concentration (10% w/v), PEGCL-I-25 vs. PEGCL-I-50, CHX release pattern from the copolymer with the lower PEG content (PEGCL-I-50) showed a much-reduced burst effect and more sustained drug release attaining completion in more than 42 days. Faster release of CHX from PEGCL-I-25 NFs can be attributed to the lower copolymer MW as well as higher bulk hydrophilicity and biodegradability of their polymer matrix (Figure 5 A and B, respectively). Such factors tend to promote intrusion of water molecules into the matrix and leaching of the drug into the release medium [46, 47].

Much faster release of CHX from PEGCL-I-50 than PEGCL-II-50 NFs despite lower copolymer concentration (5 % w/v) and higher MW of the PEG segment (4300) of PEGCL-II-50 NFs can be explained by the lower copolymer MW and greater hydrophilicity of PEGCL-I-50 (Table 3). A comparison of the release data for PEGCL-II-25 and PEGCL-II-50 with a similar polymer concentration (5% w/v) indicated faster release of the former despite higher hydrophilicity and biodegradability of the latter (Table 3), pointing to the major role played by the polymer MW in drug delivery by NFs.

Burst release, a common drawback of nanofibrous drug delivery scaffolds, can be addressed by different strategies [57]. In the present study, modulation of the copolymer MW and hydrophilicity allowed to achieve a spectrum of multi-hour to multi-day CHX release profiles suitable for early short-term effects at higher drug concentrations and more sustained effects, respectively.

On the other hand, CHX release from NFs at pH 4.4 (Figure 9B) was generally monophasic and much faster than its release at physiological pH. Data showed a similar but less obvious

DOI: 10.62184/tpdd.jtpdd110020241

dependence on copolymer MW and was almost complete during the 6 hour-study period. Results can be explained by the higher solubility of CHX at a lower pH of the acetate buffer upon penetration into the porous core/shell copolymer NFs structure via the more hydrophilic shell. Results pointed to the crucial role of the release medium in relation to drug solubility in addition to the NFs-related properties in modifying drug release kinetics.

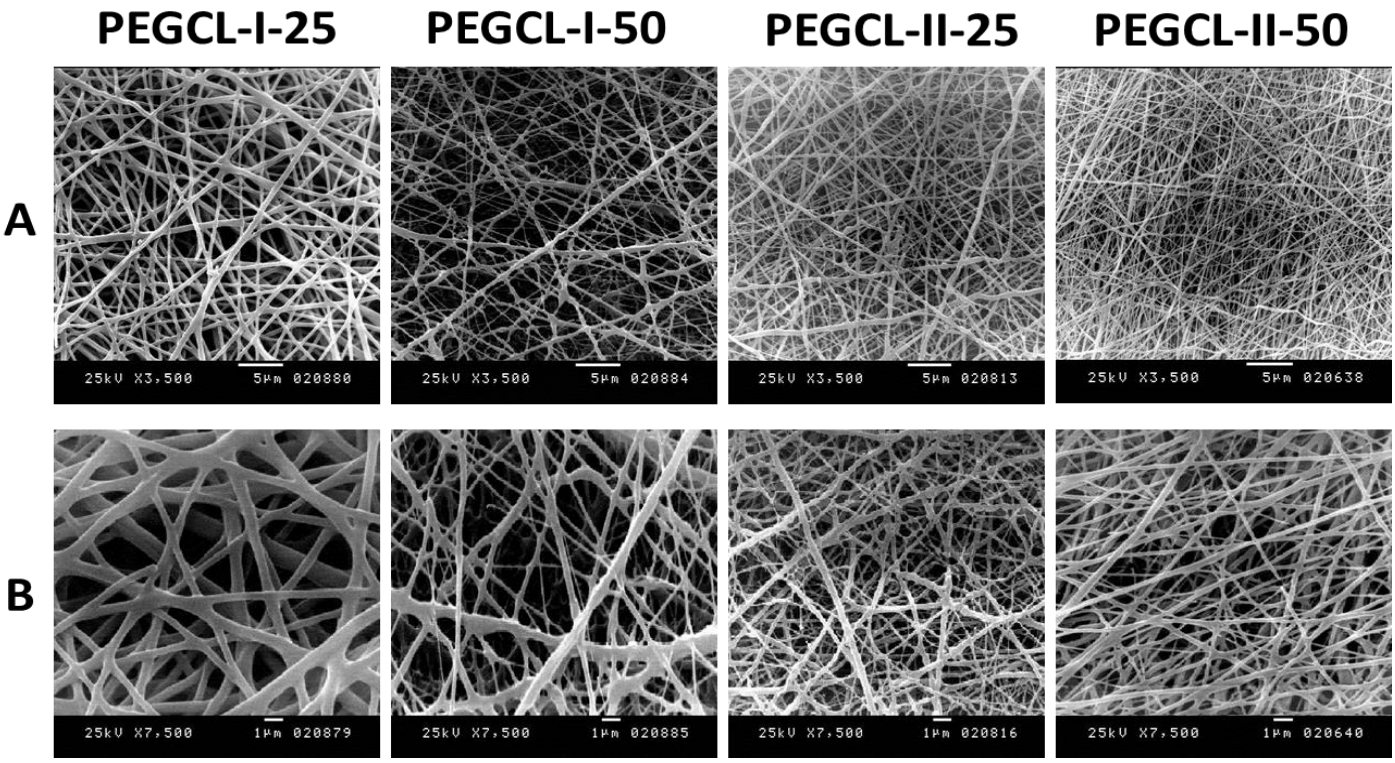

Figure 7. SEM of chlorhexidine-loaded copolymer nanofibers at two magnifications: (A) x 3500 and (B) x7500.

Table 3. Physicochemical properties of plain and 0.5% chlorhexidine loaded copolymer nanofibers.

Copolymer			**Plain copolymer nanofibers**			**CHX-copolymer nanofibers**		
Type	MW	% w/v	Mean diameter nm± SD	% Water uptake, 6 hours	% Wt loss, 15 days	Mean diameter nm± SD	EE%	% CHX release at 2 days at pH 7.4± SD (n=3)
PEGCL-I-25	212500	10	108±63	150	43	205±11	84.3	43.6±1.98
PEGCL-I-50	85460	10	92±14	170	56	169±44	77.3	98.0±2.48
PEGCL-II-25	119160	5	117±36	180	43	192±62	80.0	59.7±1.82
PEGCL-II-50	338300	5	117±38	230	56	163±68	85.4	42.0±2.41

DOI: 10.62184/tpdd.jtpdd110020241

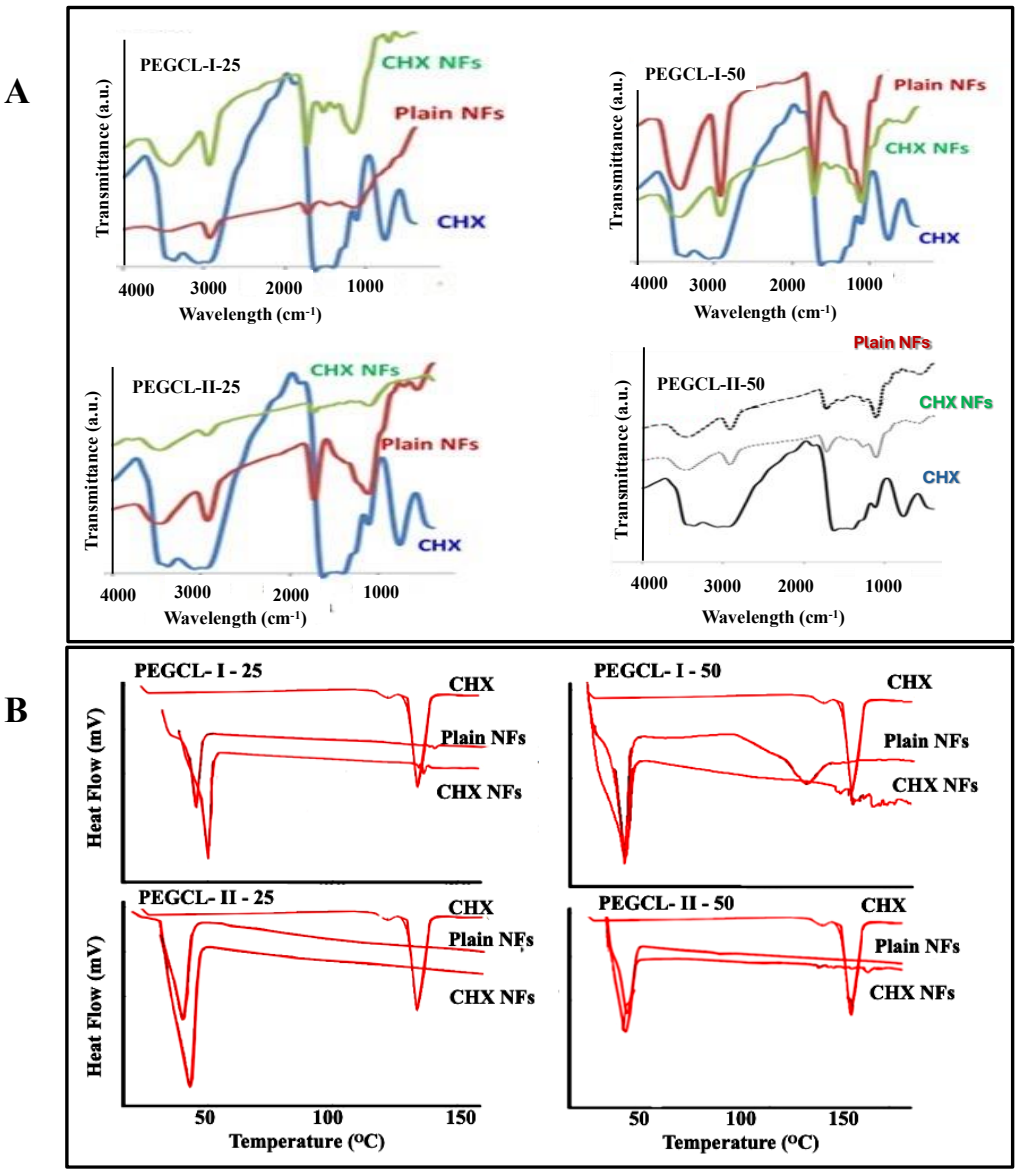

Figure 8. Solid state properties of chlorhexidine-NFs: (A) FT-IR spectra and (B) DSC curves of CHX-NFs and their CHX and plain copolymer components.

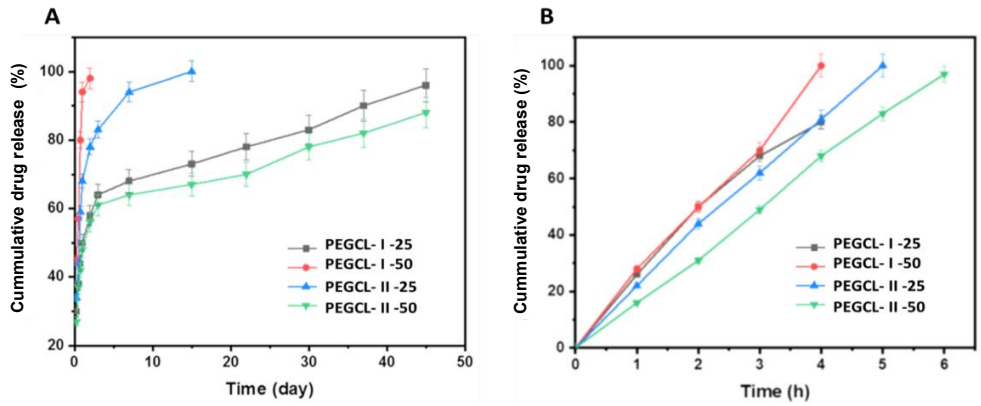

Figure 9. Chlorhexidine release profiles at: (A) pH 7.4 and (B) pH 4 at 37°C.

Accordingly, the synthesized amphiphilic block copolymers as electrospinning matrices allowed the delivery of entrapped CHX at different rates in response to the copolymer composition and the medium pH change. Thus, copolymers provide an effective means of controlling CHX release from NFs and possibly other copolymer structures, corroborating literature data [46, 58].

4. Conclusion

Amphiphilic biodegradable polyurethane copolymers as electrospinning polymer matrices for sustaining the delivery were synthesized chlorhexidine in diverse biomedical applications. A series of chlorhexidine-based antimicrobial nanofibers with customizable physicochemical and drug-release properties were developed. Interplay of the molecular weight of the copolymers and their water uptake capacity and biodegradability as well as molecular distribution of the drug in the hydrophobic segments of NFs without chemical interaction proved to be the key determinants of CHX release patterns and their responsiveness to the medium pH. A major outcome of the study was the modulation of CHX release to generate a relatively wide spectrum of release profiles at physiological pH featuring fast burst release with relatively short term multi-hour sustained effect as well as reduced burst associated with a considerably longer multi-day sustained release phase extending over more than 42 days. The CHX/copolymer nanofibers provide a platform of non-antibiotic nanofibrous scaffolds for both short-term and long-term antimicrobial biomedical applications such as those involving local or superficial infections, operative sites in dental or other surgeries as well as coating of medical devices.

Declaration of Interest Statement

The authors declare that this work has not been done or published before and has no competing financial interests.

Author Contributions

Hend Ramadan contributed to methodology, data analysis, and drafting of the manuscript. Sherif Kandil, Labiba El-Khordagui and Ahmed Abdel-Fattah contributed to conceptualization, supervision, and manuscript editing.

Supplementary Information

Supplementary file to this article can be found online at https://doi.org/10.62184/tpdd.jtpdd110020241

Author Information

Corresponding Author: Ahmed Abd El-Fattah*

Email: abdelfattah@alexu.edu.eg

ORCID iD: 0000-0002-9282-8504

Authors' ORCID iD:

Labiba El-Khordagui 0000-0002-6607-8113

Sherif Kandil 0000-0003-2249-0808

References

[1] Walsh, T. R., Gales, A. C., Laxminarayan, R., & Dodd, P. C. (2023). Antimicrobial resistance: addressing a global threat to humanity. Plos Medicine, 20(7), e1004264. https://doi.org/10.1371%2Fjournal.pmed.1004264

[2] Al-Aizari, F. A., Ghabbour, H. A., Kheder, N. A., Soliman, S. M., Hassan, M. Z., Tasqeeruddin, S., & Mabkhot, Y. N. (2024). Synthesis, X-ray structure analysis, computational investigations, and in vitro biological evaluation of new thiazole-based heterocycles as possible antimicrobial agents. Polycyclic Aromatic Compounds, 44(5), 1-14. https://doi.org/10.1080/10406638.2023.2172053

[3] Yılmaz, G. E., Göktürk, I., Ovezova, M., Yılmaz, F., Kılıç, S., & Denizli, A. (2023). Antimicrobial nanomaterials: a review. Hygiene, 3(3), 269-290. https://doi.org/10.3390/hygiene3030020

[4] Li, S., Jiang, S., Jia, W., Guo, T., Wang, F., Li, J., & Yao, Z. (2024). Natural antimicrobials from plants: recent advances and future prospects. Food Chemistry, 432, 137231. https://doi.org/10.1016/j.foodchem.2023.137231

[5] Sukmarini, L., Atikana, A., & Hertiani, T. (2024). Antibiofilm activity of marine microbial natural products: potential peptide- and polyketide-derived molecules from marine microbes toward targeting biofilm-forming pathogens. Journal of Natural Medicine, 78(1), 1-20. https://doi.org/10.1007/s11418-023-01754-2

[6] Zhang, X., Song, Y., Zhang, Z., Lu, C., & Shen, Y. (2024). New bioactive secondary metabolites from the soil-derived streptomyces sp. S045 and their anti-bacterial and anti-type III secretion system activities. Natural Product Research, 1-7. https://doi.org/10.1080/14786419.2024.2306601

[7] Houari, A., & Di Martino, P. (2007). Effect of chlorhexidine and benzalkonium chloride on bacterial biofilm formation.

Letters in Applied Microbiology, 45(6), 652-656. https://doi.org/10.1111/j.1472-765X.2007.02249.x

[8] Aftab, R., Dodhia, V. H., Jeanes, C., & Wade, R. G. (2023). Bacterial sensitivity to chlorhexidine and povidone-iodine antiseptics over time: a systematic review and meta-analysis of human-derived data. Scientific Reports, 13(1), 1-6. https://doi.org/10.1038/s41598-022-26658-1

[9] Bednarek, R. S., Nassereddin, A., & Ramsey, M. L. (2024). Skin antiseptics. In StatPearls. https://www.ncbi.nlm.nih.gov/pubmed/29939630

[10] Azzopardi, A., & Trapani, J. (2024). Chlorhexidine-based versus non-chlorhexidine dressings to prevent catheter-related bloodstream infections: an evidence-based review. Nursing in Critical Care, 29(1), 191-195. https://doi.org/10.1111/nicc.12879

[11] Graves, N., Gardner, A., Collignon, P., Koerner, J., Gregory, V., Cheng, A., Fasugba, O., & Mitchell, B. G. (2019). Chlorhexidine versus saline in reducing the risk of catheter associated urinary tract infection: a cost-effectiveness analysis. International Journal of Nursing Studies, 97, 1-6. https://doi.org/10.1016/j.ijnurstu.2019.04.003.

[12] Satpute, T. S., & Mulay, S. A. (2021). Chlorhexidine in operative dentistry - A Review. Journal of the International Clinical Dental Research Organization, 13(2) 80-85. https://doi.org/ 10.4103/jicdro.jicdro_2_21

[13] Katle, E., Zandi, H., Pedersen, D., Sunde, P. T., Torgersen, G. R., & Ørstavik, D. (2024). Radiographic outcome of endodontic treatment and retreatment of teeth with apical periodontitis using two different root canal irrigants. a prospective cohort study. International Endodontic Journal, 57(3), 297-304. https://doi.org/10.1111/iej.14019

[14] Mensitieri, F., Caggiano, M., Gaudino, G., Charlier, B., Coglianese, A., Amato, A., Di Spirito, F., Amato, M., Dal Piaz, F., & Izzo, V. (2023). In vitro evaluation of antibacterial and antibiofilm activity of different chlorhexidine-containing mouthwash formulations against streptococcus mutans. Applied Sciences, 13(13) 1-15. https://doi.org/10.3390/app13137531

[15] Waqar, S. M., Razi, A., Qureshi, S. S., Saher, F., Zaidi, S. J. A., & Kumar, C. (2024). Comparative evaluation of propolis mouthwash with 0.2% chlorhexidine mouthwash as an adjunct to mechanical therapy in improving the periodontitis among perimenopausal women: a randomized controlled trial. BMC Oral Health, 24(1), 26. http://doi.org/10.1186/s12903-023-03768-4

[16] Hussien, s. a., & Hamdi, N. A. (2024). Effect of new delivery method on antibacterial properties of chlorohexidine (in-vitro study). Egyptian Dental Journal, 70(1), 707-713. https://doi.org/10.21608/edj.2023.213683.2570

[17] Lima, I. S. d., Silva, A. S., Nascimento, A. M. S. S., de Oliveira, L. H., Morais, A. Í. S., Barreto, H. M., Peña-Garcia, R., Cuevas, M. D. M. O., Argôlo Neto, N. M., Osajima, J. A., Muniz, E. C., & da Silva-Filho, E. C. (2024). Synthesis and characterization of cassava gum hydrogel associated with chlorhexidine and evaluation of release and antimicrobial activity. Macromolecular Bioscience, 24(6), 2300507. https://doi.org/10.1002/mabi.202300507

[18] Rai, V. K., Kumar, A., Pradhan, D., Halder, J., Rajwar, T. K., Sarangi, M. K., Dash, P., Das, C., Manoharadas, S., Kar, B., Ghosh, G., & Rath, G. (2024). Spray-dried mucoadhesive re-dispersible gargle of chlorhexidine for improved response against throat infection: formulation development, in vitro and in vivo evaluation. American Association of Pharmaceutical Scientists, 25(2), 31. https://doi.org/10.1208/s12249-024-02750-9

[19] Al Thaher, Y., Abdelghany, S., & Abulateefeh, S. R. (2024). pH-responsive LBL coated silica nanocarriers for controlled release of chlorhexidine. Colloids and Surfaces A: Physicochemical and Engineering Aspects, 680, 132671. https://doi.org/10.1016/j.colsurfa.2023.132671

[20] Wang, S., Fang, L., Zhou, H., Wang, M., Zheng, H., Wang, Y., Weir, M. D., Masri, R., Oates, T. W., Cheng, L., Xu, H. H. K., & Liu, F. (2024). Silica nanoparticles containing nano-silver and chlorhexidine respond to pH to suppress biofilm acids and modulate biofilms toward a non-cariogenic composition. Dental Materials, 40(2), 179-189. https://doi.org/10.1016/j.dental.2023.11.006

[21] Alansari, N., Abid, M., & Dziedzic, A. (2024). Enhanced antimicrobial efficacy of chlorhexidine-encapsulated halloysite nanotubes incorporated in presurgical orthopedic appliances: an in vitro, controlled study. Clinical Oral Investigations, 28(1), 68. https://doi.org/10.1007/s00784-023-05464-7

[22] Venmathi Maran, B. A., Jeyachandran, S., & Kimura, M. (2024). A review on the electrospinning of polymer nanofibers

and its biomedical applications. Journal of Composites Science, 8(1) 1-19. https://doi.org/10.3390/jcs8010032

[23] Kajdič, S., Planinšek, O., Gašperlin, M., & Kocbek, P. (2019). Electrospun nanofibers for customized drug-delivery systems. Journal of Drug Delivery Science and Technology, 51, 672-681. https://doi.org/10.1016/j.jddst.2019.03.038

[24] De Carvalho, L. D., Peres, B. U., Shen, Y., Haapasalo, M., Maezono, H., Manso, A. P., Ko, F., Jackson, J., & Carvalho, R. M. (2023). Chlorhexidine-containing electrospun polymeric nanofibers for dental applications: an in vitro study. Antibiotics, 12(9) 1-12. https://dx.doi.org/10.3390/antibiotics12091414

[25] Chen, X., Liu, Z., Ma, R., Lu, J., & Zhang, L. (2024). Electrospun nanofibers applications in caries lesions: prevention,ment and regeneration [10.1039/D3TB02616G]. Journal of Materials Chemistry B, 12(6), 1429-1445. https://doi.org/10.1039/D3TB02616G

[26] Kececiler-Emir, C., Basaran-Elalmis, Y., Sahin, Y. M., Bulus, E., & Yucel, S. (2023). Fabrication and characterization of chlorhexidine gluconate loaded poly(vinyl alcohol)/45S5 nano-bioactive glass nanofibrous membrane for guided tissue regeneration applications. Biopolymers, 114(10), e23562. https://doi.org/10.1002/bip.23562

[27] Kan, Y., Bondareva, J. V., Statnik, E. S., Koudan, E. V., Ippolitov, E. V., Podporin, M. S., Kovaleva, P. A., Kapaev, R. R., Gordeeva, A. M., Cvjetinovic, J., Gorin, D. A., Evlashin, S. A., Salimon, A. I., Senatov, F. S., & Korsunsky, A. M. (2023). Hydrogel-inducing graphene-oxide-derived core-shell fiber composite for antibacterial wound dressing. International Journal of Molecular Sciences, 24(7) 1-20. https://doi.org/10.3390/ijms24076255

[28] Pouponneau, P., Perrey, O., Brunon, C., Grossiord, C., Courtois, N., Salles, V., & Alves, A. (2020). Electrospun bioresorbable membrane eluting chlorhexidine for dental implants. Polymers, 12(1) 1-19. https://doi.org/10.3390/polym12010066.

[29] Chen, Z.-J., Lv, J.-C., Wang, Z.-G., Wang, F.-Y., Huang, R.-H., Zheng, Z.-L., Xu, J.-Z., & Wang, J. (2022). Polycaprolactone Electrospun nanofiber membrane with sustained chlorohexidine release capability against oral pathogens. Journal of Functional Biomaterials, 13(4), 280. https://doi.org/10.3390/jfb13040280

[30] Wali, A., Zhang, Y., Sengupta, P., Higaki, Y., Takahara, A., & Badiger, M. V. (2018). Electrospinning of non-ionic cellulose ethers/polyvinyl alcohol nanofibers: characterization and applications. Carbohydrate Polymers, 181, 175-182. https://doi.org/10.1016/j.carbpol.2017.10.070

[31] Kasbiyan, H., Yousefzade, O., Simiand, E., Saperas, N., Del Valle, L. J., & Puiggali, J. (2022). Antibacterial hydrogels derived from poly(gamma-glutamic acid) Nanofibers. Gels, 8(2), 120. https://doi.org/10.3390/gels8020120

[32] Hassiba, A. J., El Zowalaty, M. E., Webster, T. J., Abdullah, A. M., Nasrallah, G. K., Khalil, K. A., Luyt, A. S., & Elzatahry, A. A. (2017). Synthesis, characterization, and antimicrobial properties of novel double layer nanocomposite electrospun fibers for wound dressing applications. International Journal of Nanomedicine, 12, 2205-2213. https://doi.org/10.2147/IJN.S123417

[33] Said, S. S., Eltaher, H. M., & El-Khordagui, L. K. (2019). Biomedical applications of composite resorbable fibers. Materials for Biomedical Engineering, 127-155. Elsevier. https://doi.org/http://dx.doi.org/10.1016/B978-0-12-818415-8.00005-X

[34] Ghasemiyeh, P., & Mohammadi-Samani, S. (2021). Polymers blending as release modulating tool in drug delivery. Frontiers in Materials, 8, 1-12. https://doi.org/10.3389/fmats.2021.752813

[35] Perumal, G., Anusree, V. S., Ravi, P., Vedanayagam, S., & Doble, M. (2024). LDPE/PCL nanofibers embedded chlorhexidine diacetate for potential antimicrobial applications. Materials Today Communications, 38, 107652. https://doi.org/10.1016/j.mtcomm.2023.107652

[36] Cometa, S., Bartolozzi, I., Corti, A., Chiellini, F., De Giglio, E., & Chiellini, E. (2010). Hydrolytic and microbial degradation of multi-block polyurethanes based on poly(ε-caprolactone)/poly(ethylene glycol) segments. Polymer Degradation and Stability, 95(10), 2013-2021. https://doi.org/10.1016/j.polymdegradstab.2010.07.007

[37] Chrószcz-Porębska, M. W., Barszczewska-Rybarek, I. M., Kazek-Kęsik, A., & Ślęzak-Prochazka, I. (2023). Cytotoxicity and microbiological properties of copolymers comprising quaternary ammonium urethane-dimethacrylates with bisphenol a glycerolate dimethacrylate and triethylene glycol dimethacrylate. Materials (Basel), 16(10), 3855. https://doi.org/10.3390/ma16103855

[38] Langwald, S. V., Ehrmann, A., & Sabantina, L. (2023). Measuring physical properties of electrospun nanofiber mats for different biomedical applications. Membranes, 13(5), 488. https://doi.org/10.3390/membranes13050488

[39] Yu, S., Zhang, Y., Hu, H., Li, J., Zhou, W., Zhao, X., & Peng, S. (2022). Effect of maleic anhydride grafted poly (lactic acid) on rheological behaviors and mechanical performance of poly (lactic acid)/poly (ethylene glycol)(PLA/PEG) blends. RSC advances, 12(49), 31629-31638. https://doi.org/10.1039/D2RA03513H

[40] Singh, I., Samal, S. K., Mohanty, S., & Nayak, S. K. (2020). Recent advancement in plant oil derived polyol-based polyurethane foam for future perspective: a review. European journal of lipid science and technology, 122(3), 1900225. https://doi.org/10.1002/ejlt.201900225

[41] Qindeel, M., Ahmed, N., Shah, K. U., & Ullah, N. (2020). New environment friendly approach for synthesis of amphiphilic PCL–PEG–PCL triblock copolymer: an efficient carrier for fabrication of nanomicelles. Journal of Polymers and the Environment, 28, 1237-1251. https://doi.org/10.1007/s10924-020-01683-1

[42] Behl, A., Parmar, V. S., Malhotra, S., & Chhillar, A. K. (2020). Biodegradable diblock copolymeric PEG-PCL nanoparticles: Synthesis, characterization and applications as anticancer drug delivery agents. Polymer, 207, 122901. http://doi.org/10.1016/j.polymer.2020.122901

[43] Matxinandiarena, E., Múgica, A., Tercjak, A., Ladelta, V., Zapsas, G., Hadjichristidis, N., Cavallo, D., Flores, A., & Müller, A. J. (2021). Sequential crystallization and multicrystalline morphology in PE-b-PEO-b-PCL-b-PLLA tetrablock quarter polymers. Macromolecules, 54(15), 7244-7257. https://doi.org/10.1021/acs.macromol.1c01186

[44] Liu, L., & Lei, L. (2023). Contact angle on rough curved surfaces and its implications in porous media. Langmuir, 39(12), 4507-4517. https://doi.org/10.1021/acs.langmuir.3c00213

[45] Gorna, K., & Gogolewski, S. (2002). In vitro degradation of novel medical biodegradable aliphatic polyurethanes based on ϵ-caprolactone and Pluronics® with various hydrophilicities. Polymer Degradation and Stability, 75(1), 113-122. https://doi.org/10.1016/S0141-3910(01)00210-5

[46] Shababdoust, A., Zandi, M., Ehsani, M., Shokrollahi, P., & Foudazi, R. (2020). Controlled curcumin release from nanofibers based on amphiphilic-block segmented polyurethanes. International Journal of Pharmaceutics, 575, 118947. https://doi.org/10.1016/j.ijpharm.2019.118947

[47] Zamani, T. (2021). Release mechanisms for profen-loaded nanofibers: challenges and opportunities. Journal of advanced Biomedical and Pharmaceutical Sciences, 4(4), 195-213. https://dx.doi.org/10.21608/jabps.2021.72197.1126

[48] de Carvalho, L. D., Peres, B. U., Shen, Y., Haapasalo, M., Maezono, H., Manso, A. P., Ko, F., Jackson, J., & Carvalho, R. M. (2023). Chlorhexidine-containing electrospun polymeric nanofibers for dental applications: an in vitro study. Antibiotics, 12(9), 1414. https://doi.org/10.3390/antibiotics12091414

[49] Zeng, J., Yang, L., Liang, Q., Zhang, X., Guan, H., Xu, X., Chen, X., & Jing, X. (2005). Influence of the drug compatibility with polymer solution on the release kinetics of electrospun fiber formulation. Journal of Control Release, 105(1-2), 43-51. https://doi.org/10.1016/j.jconrel.2005.02.024

[50] Huynh, T. T., Padois, K., Sonvico, F., Rossi, A., Zani, F., Pirot, F., Doury, J., & Falson, F. (2010). Characterization of a polyurethane-based controlled release system for local delivery of chlorhexidine diacetate. European journal of pharmaceutics and biopharmaceutics, 74(2), 255-264. https://doi.org/10.1016/j.ejpb.2009.11.002

[51] Bettencourt, A. F., Costa, J., Ribeiro, I. A. C., Gonçalves, L., Arias-Moliz, M. T., Dias, J. R., Franco, M., Alves, N. M., Portugal, J., & Neves, C. B. (2023). Development of a chlorhexidine delivery system based on dental reline acrylic resins. International Journal of Pharmaceutics, 631, 122470. https://doi.org/10.1016/j.ijpharm.2022.122470

[52] Cortés, M. E., Sinisterra, R. D., Avila-Campos, M. J., Tortamano, N., & Rocha, R. G. (2001). The chlorhexidine: beta;-cyclodextrin inclusion compound: preparation, characterization and microbiological evaluation. Journal of inclusion phenomena and macrocyclic chemistry, 40, 297-302. http://doi.org/10.1023/A:1012788432106

[53] Pupe, C. G., Villardi, M., Rodrigues, C. R., Rocha, H. V. A., Maia, L. C., de Sousa, V. P., & Cabral, L. M. (2011). Preparation and evaluation of antimicrobial activity of nanosystems for the control of oral pathogens Streptococcus mutans and Candida albicans.

International Journal of Nanomedicine, 6, 2581-2590. https://doi.org/10.2147/IJN.S25667

[54] El-Shattawy, H. H. (1984). Nalidixic acid-direct compression excipients, preformulation stability screening using differential scanning calorimetry. Drug Development and Industrial Pharmacy, 10(3), 491-504. http://doi.org/10.3109/03639048409041402

[55] Ono, S., Imai, R., Ida, Y., Shibata, D., Komiya, T., & Matsumura, H. (2015). Increased wound pH as an indicator of local wound infection in second degree burns. Burns, 41(4), 820-824. https://doi.org/10.1016/j.burns.2014.10.023

[56] Gaydhane, M. K., Sharma, C. S., & Majumdar, S. (2023). Electrospun nanofibres in drug delivery: advances in controlled release strategies. RSC Advances, 13(11), 7312-7328. https://doi.org/10.1039/d2ra06023j

[57] Chou, S.-F., Carson, D., & Woodrow, K. A. (2015). Current strategies for sustaining drug release from electrospun nanofibers. Journal of Controlled Release, 220, 584-591. https://doi.org/10.1016/j.jconrel.2015.09.008

[58] Gao, Y., Bach Truong, Y., Zhu, Y., & Louis Kyratzis, I. (2014). Electrospun antibacterial nanofibers: Production, activity, and in vivo applications. Journal of Applied Polymer Science, 131(18), 40797. https://doi.org/10.1002/app.40797